Multiaxial Deformation of Polymer Networks

Yves Termonia

Central Research and Development, Experimental Station, E. I. du Pont de Nemours, Inc., Wilmington, Delaware 19898

Received June 15, 1990; Revised Manuscript Received September 12, 1990

ABSTRACT: We have developed a detailed molecular model for describing the response of a polymer network to multiaxial deformation. The approach allows one to explicitly calculate the strain energy density function W and its dependence on the strain invariants I. The results correctly describe the peculiar behavior of the strain energy derivatives observed experimentally at very low deformation and at high strains. The strong dependence of those derivatives on strain is attributed to slippage of molecular chains through entanglements. Our model predictions also clearly demonstrate the lack of physical meaning associated with the phenomenological Mooney–Rivlin equation.

1. Introduction

A complete understanding of the behavior of polymers under multiaxial deformation is a very complex problem of great experimental as well as theoretical interest. Rubberlike materials are ideal candidates for those studies because of their large extensibility and weak time dependence of their stress–strain curves. The deformation of those materials has been usually described in terms of the strain energy density function, W.[1] That function plays in continuum mechanics a role equally as important as that of the free energy in thermodynamics. Thus, a knowledge of the dependence of W on strain allows a complete determination of the state of stress at any given point in a deformed body. Also, the precise form of the energy density function for polymeric materials must be obtained from a detailed molecular study of the effect of deformation on the macromolecular chains, just as the determination of the free energy functional for a ferromagnet cannot be derived from classical thermodynamics and requires a separate model for the local fields acting on a single atom.

Several models have been proposed for describing the dependence of the energy density on strain for rubberlike materials. The phenomenological approach of Rivlin and Saunders[2] led to the first constitutive relation for W. Some alternative semiempirical relationships were proposed more recently.[3-5] Other researchers have focused on more comprehensive models looking in detail into the effects of entanglements on deformation behavior. These models can be grouped into four categories: constrained fluctuation,[6] primitive path,[7,8] sliplink,[9,10] and tube[11,12] models. The relative merits of these various approaches in fitting experimental data on biaxial deformation have been recently reviewed by Gottlieb and Gaylord.[13] None of the models, however, was found to be successful in predicting experimental observation over the entire range of investigation.

In a recent series of publications,[14-16] we introduced a network model for the study of the mechanical properties of cross-linked elastomers. The model explicitly takes into account the role of entanglements latent in the polymer prior to cross-linking. It also allows for chain slippage through a detailed analysis of the force gradients near entanglement points. For simplicity, however, the approach was restricted to uniaxial testing. It is extended here to multiaxial deformation in an attempt to isolate the effects of entanglements on the form of the strain energy density function.

2. Model

The basic features of the model have been described at length in ref 14. Here, we will limit ourselves to summarize the essential features that are of relevance in an extension of our approach to multiaxial deformation.

Figure 1 describes our model setup for biaxial deformation of polymer networks. The network in Figure 1 was obtained[14] through end-linking of difunctional polymer chains with tetrafunctional cross-links (symbol □). As in ref 14, the present work is restricted to starting polymer chains having a monodisperse molecular weight distribution with M equal to 4 times the molecular weight between entanglements, M_e. Each macromolecule in Figure 1 is thus defined through a random walk connecting three nodes (entanglements, symbol ●) on the network. That network of random walks was built by a step-by-step procedure based on scanning at each step for the possible continuations of the chains in the future steps. This allows generation of an ensemble of chains with a molecular weight distribution as close as possible to monodisperse. Details of the configuration of a molecular chain strand between entanglements are omitted in the model, and only end-to-end vectors (wiggly lines) are being considered. Upon completion of that process, the chains are cross-linked at their ends with tetrafunctional monomers, taking a degree of advancement of the reaction p equal to 0.98. Chain ends in the network have not been represented and this allows one to identify in Figure 1a the presence of several defects due to incomplete reaction ($p < 1$). The network of Figure 1a contains 31 junctions (entanglements + cross-links) in both the x and y directions. The film is assumed to be infinitesimally thin with a thickness of the order of the distance between nearest-neighbor entanglements (Figure 1b).

The film is entangled at its four sides with rigid bars which are assumed to be frictionless so that the chain "hooks" at the edges of the network are allowed to run freely on the rail bars. The corners of the film, however, are clamped in order to minimize nonuniformity of the deformation in those regions. The film is stretched biaxially along the x and y directions by displacements of two rail bars (Figure 1a) that can move back and forth through frictionless sliding joints. The forces exerted by the bars on the film lead to displacements of the network nodes in the x, y, and z directions. These displacements are calc ated by minimizing the net residual stresses acting on each of the nodes in turn. This constitutes a very computer time consuming process which has been optimized by using computational devices which consid-

0024-9297/91/2224-1128$02.50/0

erably speed up the convergence of the calculations.[17] The relaxation toward mechanical equilibrium was considered to be complete when the largest residual stress on a node fell below 0.2% of the average stress per strand. For simplicity, we do not explicitly calculate displacements of the nodes along the z direction and assume that the network junctions move affinely in that direction so as to keep the total volume constant.

The state of stress of a particular chain strand between junction nodes (entanglements or cross-links) is obtained as follows. Let r and $w(r)$ denote respectively and end-to-end vector length and free energy of deformation for that chain. The engineering stresses σ_x and σ_y along the x and y directions are given by[18]

$$\sigma_x = \partial w(r)/\partial \lambda_x = [\mathrm{d}w(r)/\mathrm{d}r][\partial r/\partial \lambda_x] \quad (1a)$$

$$\sigma_y = \partial w(r)/\partial \lambda_y = [\mathrm{d}w(r)/\mathrm{d}r][\partial r/\partial \lambda_y] \quad (1b)$$

in which λ_x and λ_y are the draw ratios along the x and y directions, respectively. Equations 1a and 1b can be rewritten in simpler form

$$\sigma_x = f[\partial r/\partial \lambda_x] \quad (2a)$$

$$\sigma_y = f[\partial r/\partial \lambda_y] \quad (2b)$$

in which

$$f = \mathrm{d}w(r)/\mathrm{d}r \quad (3)$$

is the force on the chain. The latter is obtained from

$$f = (kT/l)\mathcal{L}^{-1}(r/nl) \quad (4)$$

In eq 4, $\mathcal{L}^{-1}$ represents the inverse Langevin function whereas n and l denote respectively the number and length of the statistical segments for the chain. We take n = 22,[14] which leads, in uniaxial extension, to an elongation at break around 200%. To summarize: The local stresses acting on a chain strand are evaluated numerically from eqs 2a,b and 4. These equations are used at two different stages in our simulations: (i) in our estimation of the nodes displacements in the x and y directions (see above) and (ii) in our measurements of the forces acting on the rail bars. The latter have been obtained from the means of the tensions measured in the central 12 chains hooked to the appropriate rail (see Figure 1a).

As has been clearly demonstrated in previous applications,[14-16] a molecular approach like the present can be quite useful in elucidating the role of entanglements in controlling the deformation behavior. Thus, as in refs 14–16, our model also explicitly allows for chain slippage though entanglements. For a given value of the external strain, this process is performed until the difference in force f in the two strands of a chain separated by an entanglement falls below the entanglement friction force, f_e. The latter is left as a free parameter in the model.

A last remark is in order. Due to an incompleteness of the cross-linking reaction ($p < 1$), the network of Figure 1 contains a large number of nonpermanent entanglements which are not trapped between cross-links. A meaningful study of its mechanical properties *at elastic equilibrium* therefore requires complete removal of all those entanglements which are not independently connected to the network through four intact chain strands. The resulting network is illustrated in Figure 2.

Upon completion of the construction of the network and removal of the non-load-bearing junctions, the mechanical properties are tested by the procedure described at length in ref 14. In that procedure, the fiber is first stretched to a small strain value in the appropriate direction(s). Chains are then allowed to slip through entanglements and to break at maximum extension. After relaxation of the whole network toward mechanical equilibrium, the overall stress on the rail bars is recorded. The bars are then moved further by a small constant amount and the whole cycle of chain slippage and network relaxation processes is repeated. This leads to the generation of a complete stress–strain curve for a given

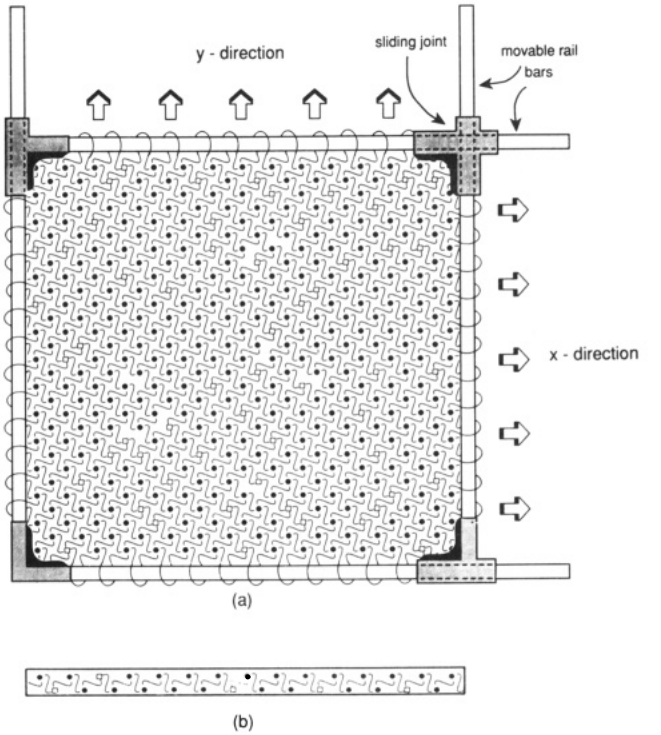

Figure 1. Model setup for biaxial deformation of polymer networks. The network was obtained through end-linking of difunctional polymer chains with tetrafunctional cross-links (symbol □). The chains have a molecular weight M close to 4 times that between entanglements, M_e, and thus have roughly 4 entanglements (symbol ●) along their contour. The degree of advancement of the cross-linking reaction is set equal to p = 0.98. Chain ends have not been represented. The network comprises 31 junctions (entanglements + cross-links) in both the x and y directions. The film is assumed to be infinitesimally thin with a thickness of the order of the distance between nearest-neighbor entanglements (shown in (b)).

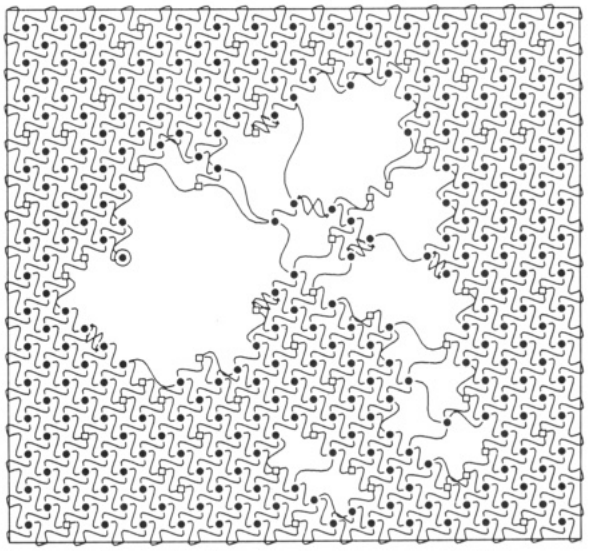

Figure 2. Network of Figure 1 after removal of the nonpermanent entanglements which are not trapped between cross-links.

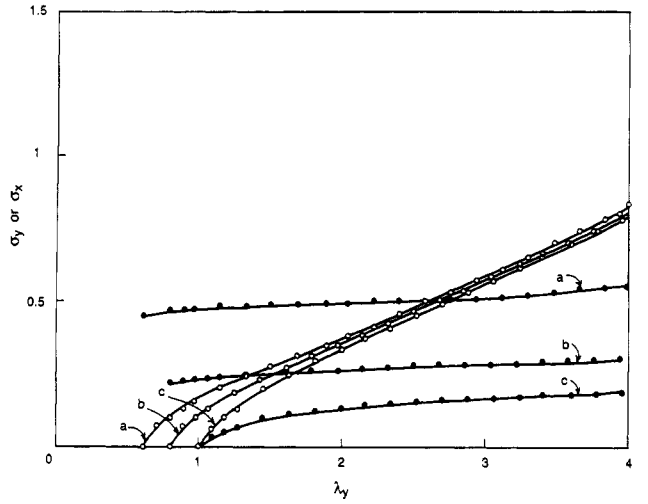

Figure 3. Calculated stress–strain curves for different values of the draw ratio λ_x in the x direction: (a) $\lambda_x = 2.68$; (b) $\lambda_x = 1.56$; (c) $\lambda_x = 1$. σ_y (○) and σ_x (●) denote the engineering stresses.

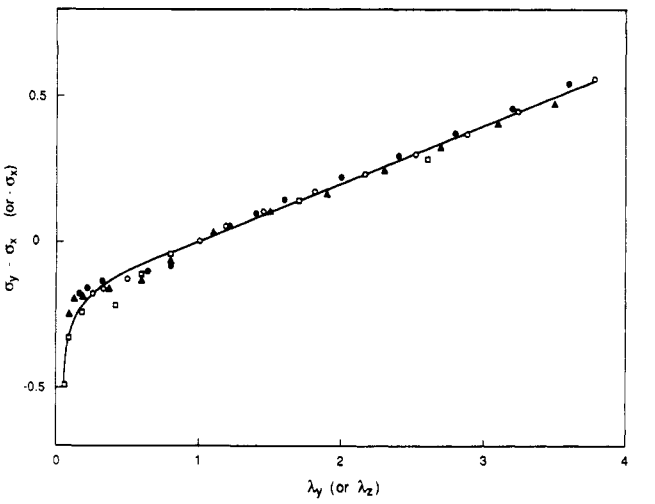

Figure 4. Jones and Treloar[19] representation of biaxial strain data. The figure shows the differences $\sigma_y - \sigma_x$ vs λ_y (or $-\sigma_x$ vs λ_z), all the curves at different λ_x being shifted vertically so as to coincide with the pure shear curve ($\lambda_x = 1$) at the point $\lambda_y = 1$. The symbols denote our calculated data for different values of λ_x: $\lambda_x = 1$ (○); $\lambda_x = 1.56$ (●); $\lambda_x = 2.68$ (▲); $\lambda_x = 6$ (□).

molecular weight M and degree of advancement of the reaction p.

3. Results and Discussion

Figure 3 shows a series of calculated stress–strain curves obtained for general biaxial deformation. In those experiments, the samples were first brought to constant and different values of the draw ratio λ_x in the x direction. They were then stretched in small increments along the y axis and the stresses σ_y and σ_x recorded. In order to facilitate the interpretation of our model results, the figure is for the case of no slippage of chains through entanglements. The results show that the σ_y curves (symbol ○) are shifted toward higher values by an increase in the initial draw λ_x. Similarly, the stress σ_x (symbol ●) measured along the x axis is seen to increase with the strain along the transverse y axis. These data thus clearly illustrate the coupling between stresses in different directions. Representation of biaxial stress data in the form of Figure 3 is, however, not very enlightening since its essential features are easily reproduced by all previous models.

An alternative representation, due to Jones and Treloar,[19] consists in plotting the differences $\sigma_y - \sigma_x$ vs λ_y (or $-\sigma_x$ vs λ_z). The curves at different λ_x are then shifted vertically so as to coincide with the pure shear curve ($\lambda_x = 1$) at the point $\lambda_y = 1$. The results are presented in Figure 4. All our data for extensions λ_x ranging from 1 to values as high as 6 are seen to fall on a single master curve, in agreement with experimental observation on rubber vulcanizates.[19] An essential feature of the Jones and Treloar representation in Figure 4 is the sharp downturn of the results at low $\lambda_y < 0.1$. That trend can be reproduced by only three[13] of the previous models: the Mooney–Rivlin equation,[2] the Edwards model,[8] and the Treloar–Riding[18] models. As previously argued in ref 18, the molecular origin of that downturn is the finite extensibility of the chains, which is explicitly taken into account in our approach through the use of an inverse Langevin expression for the stress (see eq 4 in that connection).

We now turn to our model predictions of the strain energy density function W. That study constitutes an excellent test of the validity of our approach since none of the previous existing models has been successful in fully describing the dependence of W over the whole range of deformation.[13] In theory, W can be directly obtained from numerical integration of stress with respect to strain (see eqs 1a,b). Of more importance, however, is the determination of its partial derivatives[20]

$$\frac{\partial W(I_1,I_2)}{\partial I_1} = \frac{1}{2(\lambda_y^2 - \lambda_x^2)}\left[\frac{\lambda_y^3\sigma_y}{\lambda_y^2 - (\lambda_y\lambda_x)^{-2}} - \frac{\lambda_x^3\sigma_x}{\lambda_x^2 - (\lambda_y\lambda_x)^{-2}}\right] \tag{5a}$$

$$\frac{\partial W(I_1,I_2)}{\partial I_2} = \frac{1}{2(\lambda_x^2 - \lambda_y^2)}\left[\frac{\lambda_y\sigma_y}{\lambda_y^2 - (\lambda_y\lambda_x)^{-2}} - \frac{\lambda_x\sigma_x}{\lambda_x^2 - (\lambda_y\lambda_x)^{-2}}\right] \tag{5b}$$

in which

$$I_1 = \lambda_x^2 + \lambda_y^2 + (\lambda_x\lambda_y)^{-2} \tag{6a}$$

$$I_2 = (\lambda_x\lambda_y)^2 + \lambda_x^{-2} + \lambda_y^{-2} \tag{6b}$$

The interest in those derivatives stems from the fact that they are directly related to the stress–strain curves:

(i) simple uniaxial extension ($\lambda \equiv \lambda_y = 1/\lambda_x^2$)

$$\sigma_y = 2\left(\lambda - \frac{1}{\lambda^2}\right)\left[\frac{\partial W(I_1,I_2)}{\partial I_1} + \frac{1}{\lambda}\frac{\partial W(I_1,I_2)}{\partial I_2}\right] \tag{7}$$

(ii) pure shear ($\lambda \equiv \lambda_y$, $\lambda_x = 1$)

$$\sigma_y = \frac{2}{\lambda}\left(\lambda^2 - \frac{1}{\lambda^2}\right)\left[\frac{\partial W(I_1,I_2)}{\partial I_1} + \frac{\partial W(I_1,I_2)}{\partial I_2}\right] \tag{8}$$

(iii) equibiaxial deformation ($\lambda \equiv \lambda_y = \lambda_x$)

$$\sigma_y = 2\left(\lambda - \frac{1}{\lambda^5}\right)\left[\frac{\partial W(I_1,I_2)}{\partial I_1} + \lambda^2\frac{\partial W(I_1,I_2)}{\partial I_2}\right] \tag{9}$$

Our results for $\partial W/\partial I_1$ and $\partial W/\partial I_2$ for general biaxial deformation are presented in Figures 5 and 6, respectively. In each figure, the values are plotted vs both the invariants $I_1 - 3$ (at constant I_2) and $I_2 - 3$ (at constant I_1). In contrast to the results presented in the previous figures, those of Figures 5 and 6 are for the original network of Figure 1 which thus contains a large number of entanglements not trapped between cross-links. The reason for that change is twofold. First, the evaluation of $\partial W/\partial I$ from eqs 5a and 5b is extremely sensitive to the values used for σ_x and σ_y, particularly in the small-strain regions. Measurements of the stresses must therefore be done with extreme

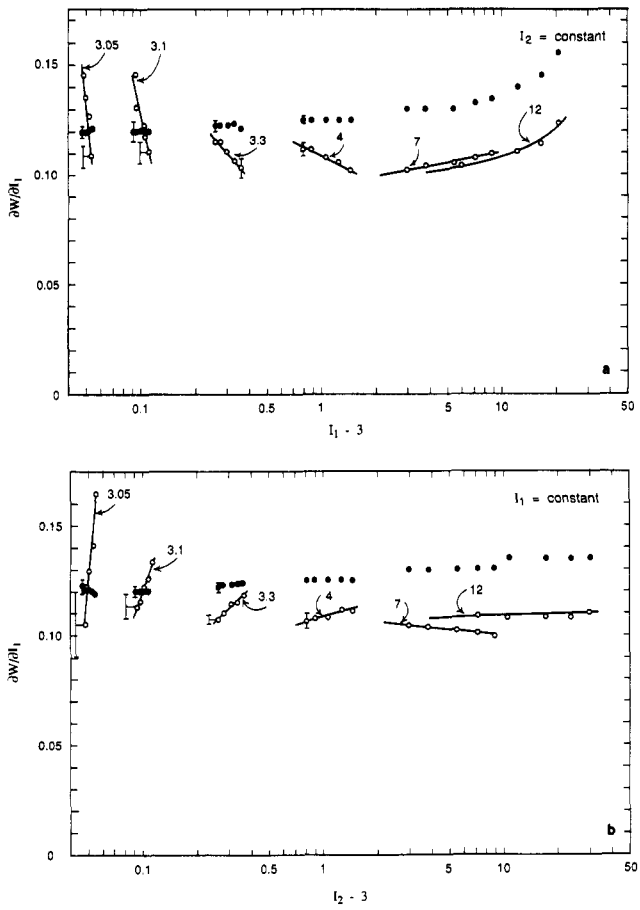

Figure 5. Strain dependence of the partial derivative $\partial W/\partial I_1$. The two sets of symbols are for results in the absence (●) and presence (○) of entanglement slippage with $f_e = 0.3$. The error bars have been estimated from the uncertainties in our σ_x and σ_y values.

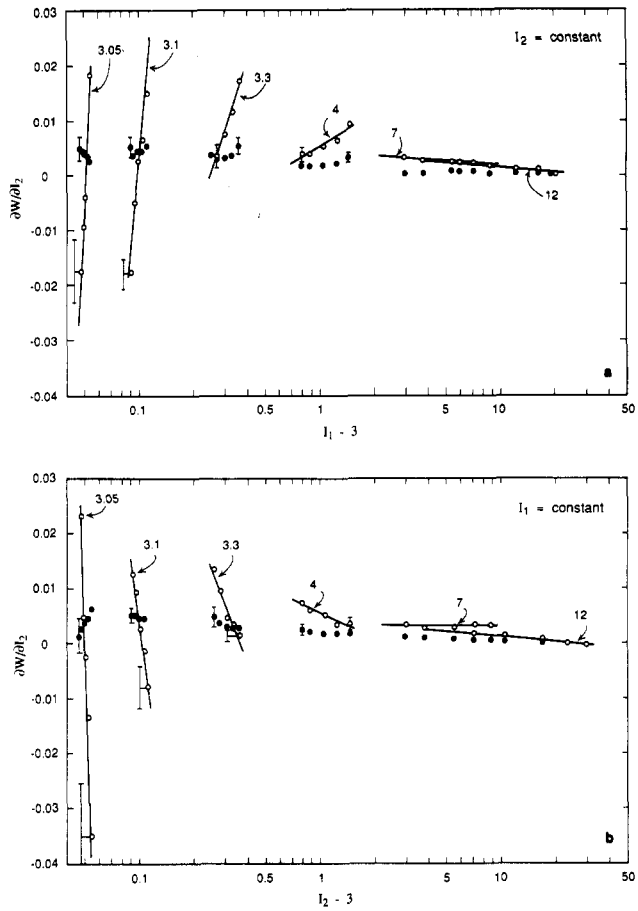

Figure 6. Strain dependence of the partial derivative $\partial W/\partial I_2$. Notation is the same as for Figure 5.

precision and care which is best ensured when the network deforms as homogeneously as possible, as in Figure 1 (compare with Figure 2). Second, it is quite likely that actual experimental samples will always contain a certain fraction of untrapped entanglements, as exemplified by the observed time dependence of the $\partial W/\partial I$'s.[20] At any rate, we do not expect the results of Figures 5 and 6 to be qualitatively affected by our simplification. Each data point in those Figures was thus obtained from a biaxial deformation of the network of Figure 1 to the required λ_x and λ_y values. Upon reaching that state, chain slippage was allowed until the difference in stress in the strands of a chain separated by an entanglement fell below an entanglement friction force f_e arbitrarily set equal to 0.3. The forces acting on the supporting bar frames were then measured and used to evaluate the $\partial W/\partial I$'s from eqs 5a and 5b. It is important to note that, when slippage is allowed, these forces will be dependent on the deformation history of the sample. This is the reason why all our results of Figures 5–9 are for a standard test in which the same starting network, i.e., that of Figure 1, is first rapidly stretched to the required λ_x and λ_y values *before* slippage through entanglements is allowed.

The range of I_1 and I_2 values covered in Figures 5 and 6 requires some explanation. For a given value of I_1, I_2 varies between a lower limit corresponding to uniaxial extension and an upper limit for equibiaxial extension. Inversely, for a given I_2, the lower and upper limits for I_1 correspond to equibiaxial and uniaxial extensions, respectively. We start by discussing our results for the case of no entanglement slippage. The data are denoted by symbol ● and have been represented together with a few typical error bars. The latter are estimated from the uncertainties in our σ_x and σ_y values. Figure 5 shows that, within experimental error, $\partial W/\partial I_1$ takes on an essentially constant value close to 0.125 (in arbitrary units) and independent of both I_1 and I_2. That value starts to increase at high deformations ($I > 6$) because of our use of an inverse Langevin function for the stress (see eq 4). Results of Figure 6 indicate a much lower value for $\partial W/\partial I_2$ which is close to zero.

Our results in the presence of entanglement slippage ($f_e = 0.3$, symbol ○) exhibit a much more complex behavior. In the limit of small strains ($I < 3.3$), $\partial W/\partial I_1$ exhibits variations as high as 60% and $\partial W/\partial I_2$ reaches negative values near equibiaxial deformation! As the strain increases, the partial derivatives become less dependent on the strain invariants and $\partial W/\partial I_2$ slowly tends toward zero. At high $I > 4$, the curves for $\partial W/\partial I_1$ change from decreasing into increasing functions of I_1. The latter is probably due to strain-hardening effects at high extensions. The complex functional form obtained in Figures 5 and 6 for the partial derivatives $\partial W/\partial I_i$ agrees in all respects with that observed experimentally by Becker[21] for natural rubber. It differs, however, from that reported in ref 20. Note also that our model is the first[13] to qualitatively reproduce the negative values of $\partial W/\partial I_2$ observed experimentally at small strains. It also clearly provides a physical interpretation of the phenomenon in terms of entanglement slippage. A similar attribution of a nonzero $\partial W/\partial I_2$ to molecular interactions has been made by Kawabata.[22]

A detailed comparison of Figures 5 and 6 also reveals that our curves for $\partial W/\partial I_1$ and $\partial W/\partial I_2$ are mirror images of each other with respect to the I axis. Figure 7 shows

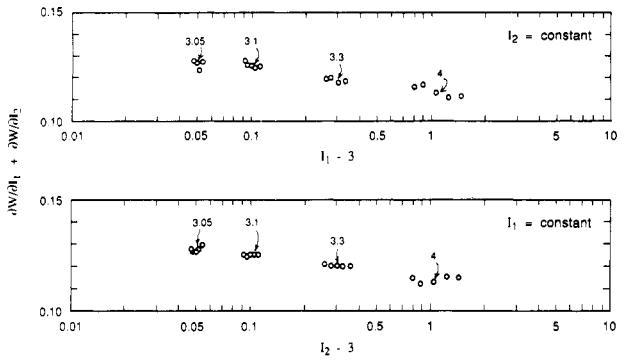

Figure 7. Strain dependence of the sum $(\partial W/\partial I_1 + \partial W/\partial I_2)$, as obtained from Figures 5 and 6.

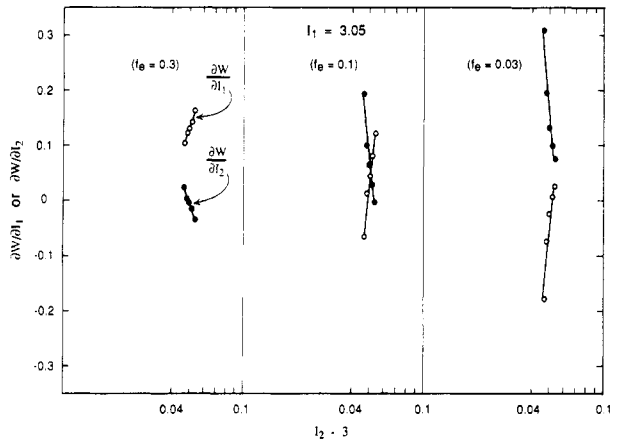

Figure 8. Strain dependence of the partial derivatives $\partial W/\partial I_1$ (○) and $\partial W/\partial I_2$ (●) for various values of the entanglement friction force f_e. Notation is the same as for Figure 5.

the strain dependence of the sum $(\partial W/\partial I_1 + \partial W/\partial I_2)$ whose value for the particular case $I_1 = I_2$ represents the modulus for the case of pure shear deformation. The figure shows that, even though the values of $\partial W/\partial I_1$ and $\partial W/\partial I_2$ separately exhibit a very complex behavior, their sum in the small-strain region ($I < 3.3$) remains essentially constant. These results, again, agree with experimental observation.[21,23]

As clearly exemplified in Figures 5 and 6, the dependence of the $\partial W/\partial I$'s on strain is due to slippage of chains through entanglements. This effect is further studied in Figure 8 in which our data for $I_1 = 3.05$ are presented for different values of the entanglement friction force f_e. The results indicate that the strain dependence of $\partial W/\partial I$ further increases at high extents of chain slippage (low f_e). The values of the derivatives themselves also exhibit a dramatically different behavior: $\partial W/\partial I_1$ goes from positive into negative values as f_e decreases whereas an opposite trend is observed with $\partial W/\partial I_2$. That very complex behavior of the $\partial W/\partial I$'s makes it very unlikely that a simple relation for their strain dependence can be found.

For the case of uniaxial deformation along the y axis, $\sigma_x = 0$ and $\lambda_x = (\lambda_y)^{-1/2}$, the partial derivatives $\partial W/\partial I_1$ and $\partial W/\partial I_2$ cannot be obtained separately from eqs 7 and their values need to be evaluated from extrapolation of the data of Figures 5 and 6. Our estimations of the $\partial W/\partial I_i$'s in pure extension (symbol ○) are presented in Figure 9 as a function of $1/\lambda$ ($\equiv 1/\lambda_y$), together with our calculated values (symbol ●) of the modulus $G/2 = [\partial W/\partial I_1 + (1/\lambda)\partial W/\partial I_2]$; see eq 7. The figure shows a linear decrease of the modulus with $1/\lambda_y$, in agreement with the Mooney–Rivlin prediction $G/2 = C_1 + (1/\lambda)C_2$.[24] However, analysis of our two contributions to the modulus also shows that $\partial W/\partial I_1$ and $\partial W/\partial I_2$ are not constant and cannot therefore be

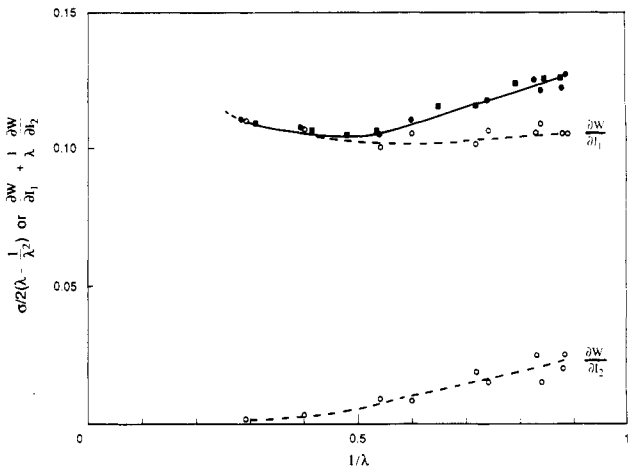

Figure 9. Mooney–Rivlin plot of modulus data for uniaxial extension. Symbol ● represents our calculated values for the sum $[\partial W/\partial I_1 + (1/\lambda)\partial W/\partial I_2]$ in which the partial derivatives (symbol ○) have been obtained by extrapolating the results of Figures 5 and 6 to uniaxial extension. Symbol ■ denotes our modulus values directly calculated from $\sigma/2(\lambda - 1/\lambda^2)$.

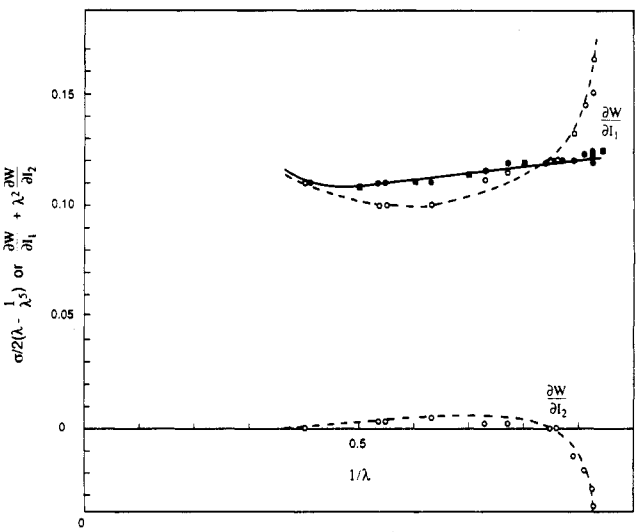

Figure 10. Mooney–Rivlin plot of modulus data for equibiaxial extension. Symbol ● represents our calculated values for the sum $[\partial W/\partial I_1 + \lambda^2\partial W/\partial I_2]$ in which the partial derivatives (symbol ○) have been obtained by extrapolating the results of Figures 5 and 6 to equibiaxial extension. Symbol ■ denotes our modulus values directly calculated from $\sigma/2(\lambda - 1/\lambda^5)$.

identified with the Mooney–Rivlin constants C_1 and C_2. Similar conclusions have been reached in previous experimental studies.[19,20] Also plotted in Figure 9 (symbol ■) are our modulus values directly calculated from $\sigma_y/2(\lambda - 1/\lambda^2)$; see eq 7. Our two sets of data for $G/2$ are in excellent agreement with each other. This, in turn, leads to strong confidence in our results of Figures 5 and 6 for the partial derivatives $\partial W/\partial I_i$.

The case of equibiaxial deformation is described in Figure 10. Again, the values of the strain derivatives (symbol ○) are not constant and exhibit a very complex behavior. In the limit of very low strains, $\partial W/\partial I_1$ shows a sharp upturn, whereas $\partial W/\partial I_2$ tends to diverge toward large negative values. However, the value of their sum in the expression for the modulus $G/2 = [\partial W/\partial I_1 + \lambda^2\partial W/\partial I_2]$ (symbol ●) (see eq 9) is essentially constant at low strains. Note that the peculiar behavior of the strain derivatives obtained here for equibiaxial deformation is quite similar to that observed experimentally by Kawabata et al.[20] for the case of uniaxial extension. The reason for that similarity in extreme types of deformation is not

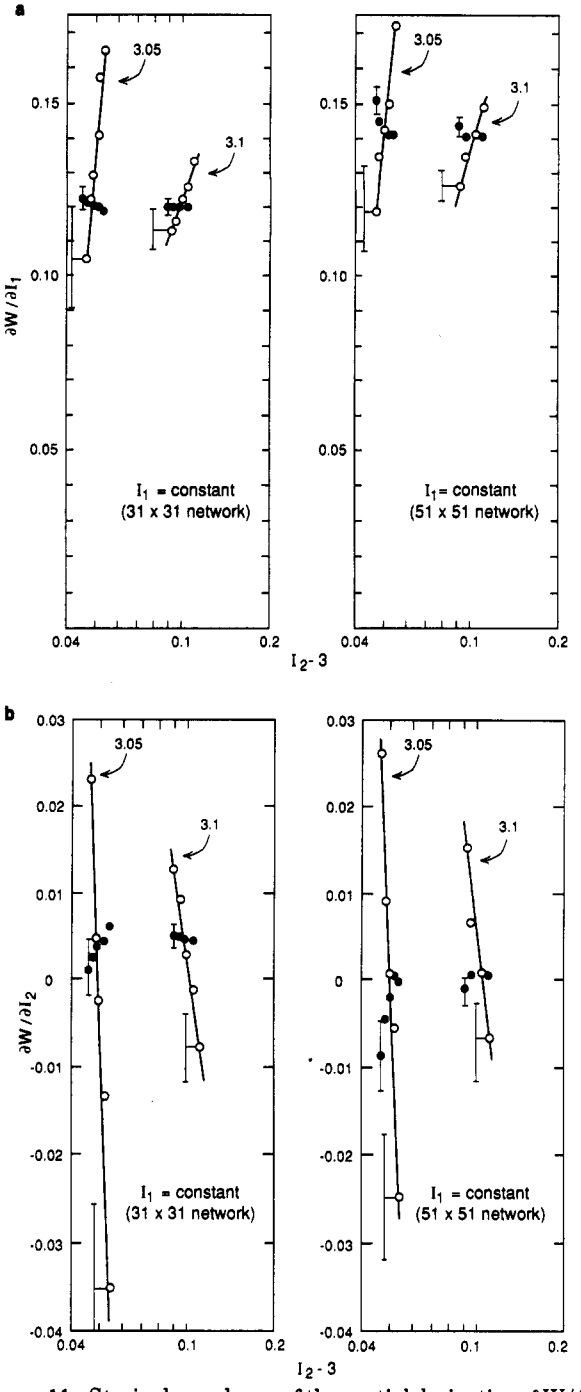

Figure 11. Strain dependence of the partial derivatives $\partial W/\partial I_1$ and $\partial W/\partial I_2$, as obtained from a small (31 × 31 junctions) and a much larger (51 × 51 junctions) network. Notation is the same as for Figure 5.

clear to us. Also represented in Figure 10 (symbol ■) are our modulus values estimated from $\sigma_y/2(\lambda - 1/\lambda^5)$; see eq 9. The good agreement between the two sets of modulus values gives further support to the validity of our results of Figures 5 and 6.

4. Conclusions

We have developed a molecular model for describing the response of a cross-linked polymer network to general biaxial deformation. The approach allows one to explicitly calculate the strain energy density function W and its dependence on the strain invariants I. Our model results are the first to correctly describe the peculiar behavior of the strain energy derivatives observed experimentally[21] at very low deformation and at high strains. The strong dependence of those derivatives on strain is attributed to slippage of molecular chains through entanglements. In view of the very complex behavior of the strain energy derivatives on model parameters, it is quite unlikely that a simple relation for their strain dependence can be found. Our model predictions also clearly demonstrate the lack of physical meaning associated with the phenomenological Mooney–Rivlin equation.

A last remark is in order. The results of the present paper have been obtained for a network of only 31 × 31 junctions. Our limitation to such small systems is due to the large amount of computer time involved in the processes of entanglement slippage and network relaxation toward mechanical equilibrium. Typically, a calculation of the $\partial W/\partial I$'s for a particular strain value requires several hours computer time on an IBM 3090. The question arises whether such small systems are representative of the behavior of actual macroscopic films. Thus, we have also made simulations on a much larger network of 51 × 51 junctions. The results for the $\partial W/\partial I$'s at constant I_1 (keeping $p = 0.98$) are presented in Figure 11 and compared to those previously obtained for the small 31 × 31 network. The $\partial W/\partial I$ values for the two networks are in quite good agreement with each other, leading to confidence in the generality of the present work. Note that the $\partial W/\partial I_1$ curves are shifted toward higher values in the large network. This is because the latter already has, prior to deformation, a smaller fraction of dangling ends. Modulus values in the absence of entanglement slippage are therefore higher and fluctuate about 0.14 (vs values around 0.125 for the small 31 × 31 network).

References and Notes

(1) Green, A. E.; Zerna, W. *Theoretical Elasticity*; Oxford University Press: London, 1954.
(2) Rivlin, R. S.; Saunders, D. W. *Philos. Trans. R. Soc. London, A* **1951**, *A243*, 251.
(3) Valanis, K. C.; Landel, R. F. *J. Appl. Phys.* **1967**, *38*, 2997.
(4) Ogden, R. W. *Proc. R. Soc. (London)* **1972**, *A326*, 565.
(5) Blatz, P. J.; Sharda, S. C.; Tschoegl, N. W. *Proc. Natl. Acad. Sci. U.S.A.* **1973**, *70*, 3041.
(6) Flory, P. J.; Erman, B. *Macromolecules* **1982**, *15*, 800.
(7) Graessley, W. W. *Adv. Polym. Sci.* **1982**, *46*, 67.
(8) Edwards, S. F. *Br. Polym. J.* **1977**, *9*, 140.
(9) Marrucci, G. *Rheol. Acta* **1979**, *18*, 193.
(10) Ball, R. C.; Doi, M.; Edwards, S. F.; Warner, M. *Polymer* **1981**, *22*, 1010.
(11) Marrucci, G. *Macromolecules* **1981**, *14*, 434.
(12) Gaylord, R. J. *Polym. Eng. Sci.* **1979**, *19*, 263.
(13) Gottlieb, M.; Gaylord, R. J. *Macromolecules* **1987**, *20*, 130.
(14) Termonia, Y. *Macromolecules* **1989**, *22*, 3633.
(15) Termonia, Y. *Macromolecules* **1990**, *23*, 1481.
(16) Termonia, Y. *Macromolecules* **1990**, *23*, 1976.
(17) Termonia, Y. *Macromolecules* **1985**, *18*, 2246.
(18) Treloar, L. R. G.; Riding, G. *Proc. R. Soc. London* **1979**, *A369*, 261.
(19) Jones, D. F.; Treloar, L. R. G. *J. Phys. D: Appl. Phys.* **1975**, *8*, 1285.
(20) Kawabata, S.; Kawai, H. *Adv. Polym. Sci.* **1977**, *24*, 89.
(21) Becker, G. W. *J. Polym. Sci., Part C* **1967**, *16*, 2893.
(22) Kawabata, S. *J. Macromol. Sci., Phys.* **1973**, *B8* (3-4), 605.
(23) Kawabata, S.; Matsuda, M.; Tei, K.; Kawai, H. *Macromolecules* **1981**, *14*, 154.
(24) Mooney, M. *J. Appl. Phys.* **1940**, *11*, 582. Rivlin, R. S. *Philos. Trans. R. Soc. London, A* **1948**, *A241*, 379.